COMPDYN 2013
4th ECCOMAS Thematic Conference on
Computational Methods in Structural Dynamics and Earthquake Engineering
M. Papadrakakis, V. Papadopoulos, V. Plevris (eds.)
Kos Island, Greece, 12–14 June 2013

NON-LINEAR DYNAMICS OF ELECTRICAL EQUIPMENT CABLES

Nicholas D. Oliveto[1] **and Mettupalayam V. Sivaselvan**[1]

[1] Department of Civil, Structural and Environmental Engineering, University at Buffalo, The State University of New York
212 Ketter Hall, Buffalo, New York 14260, USA
{noliveto, mvs}@buffalo.edu

Keywords: Cable Dynamics, Large Displacements, Large Rotations, Earthquake Excitation.

Abstract. *In power substations, electrical cables are commonly observed in configurations that cannot be explained by tension stress states only. Moreover, during extreme excitations such as earthquakes, they can be subjected to large displacements and rotations, as well as forces that can lead to failure of both the cables and the equipment to which they are connected. In this paper a three-dimensional geometrically exact beam model is presented and used to describe the static and dynamic behavior of electrical equipment cables. The model is implemented in MATLAB and applied to a flexible conductor recently tested at the SEESL laboratory at the University at Buffalo. Both static and dynamic numerical applications are performed. First the initial configuration of the tests is obtained by imposing the end displacements and rotations to a straight and unstrained cable. Then the cable is subjected to resonant harmonic out-of-plane and in-plane horizontal ground motions. Due to the high frequency components resulting from the axial response of the cable, and to the fact that the Newmark time-integration algorithm used herein generally fails to conserve energy, very small time steps are needed for the algorithm to converge. Although algorithms have been proposed in the literature, which introduce numerical damping to stabilize the computations, the introduction of real forms of damping in the model and the simulation of the dynamic experimental tests performed at the University at Buffalo are object of current work.*

1 INTRODUCTION

Cables are widely used in the power industry as essential components of the electrical transmission network. Although they are usually designed to mainly meet electrical standards rather than structural performance requirements, during earthquakes and other severe environmental hazards they are often subjected to large deformations and stresses that can result in failure of both the cables and the equipment to which they are connected. During extreme excitations the cables can undergo large displacements and rotations, and be subjected to three-dimensional states of stress. Besides tension, the cable can be subjected to shear, bending and torsion. Moreover it is common in electrical substations to observe cable configurations that cannot be explained by a state of stress of simple tension.

Dynamic interaction between cables and interconnected equipment has been studied, among others, by Der Kiureghian et al. [1] using a three-dimensional geometrically exact beam model originally proposed by Simo et al. [2,3,4]. Moreover, extensive experimental tests on flexible conductors provided by the Bonneville Power Authority have recently been conducted at the SEESL laboratory at the University at Buffalo in the form of pull-back tests, harmonic tests and shake table earthquake excitations [5].

In the present paper the theory developed by Simo and coworkers is exploited to set the stage for the simulation of the experimental tests carried out at the University at Buffalo on a Jefferson/TW AAC conductor. Of particular interest is the determination of the initial static configuration from which the dynamic tests on the cable are performed. The initial shape is obtained by imposing the end displacements and rotations to an initially straight and unstrained cable. The properties of the cable are taken so as to obtain a reasonably good match between the numerical and experimental configurations and frequencies.

The paper is organized as follows. In the first section the governing equations of the 3D geometrically exact beam model are presented, including kinematics, equilibrium and constitutive equations. The second section deals with the derivation of the weak form of the equilibrium equations. Its exact linearization and discretization in time and space then leads to the definition of a tangent operator and a system of equations solvable by means of an iterative scheme of the Newton type. The final section is concerned with static and dynamic numerical applications of an electrical cable. The results are compared where possible to those obtained from experimental tests performed at the University at Buffalo.

2 GOVERNING EQUATIONS

The purpose of this section is to describe the equations governing the motion of the three-dimensional geometrically exact beam model which will be used to model the cable.

2.1 Kinematics

Following Simo [2], the motion of the beam through time is uniquely defined by the position of the line of centroids $\mathbf{x_0}(S,t)$ and a rotation tensor $\mathbf{R}(S,t)$ specifying the orientation of a moving frame $\mathbf{t_I}(S,t)$ attached to the cross-section, relative to its initial position $\mathbf{E_I}$. The rotation tensor $\mathbf{R}(S,t)$ represents a rigid rotation of the cross-section such that

$$\mathbf{t_I}(S,t) = \mathbf{R}(S,t) \cdot \mathbf{E_I} \tag{1}$$

The derivatives of $\mathbf{R}(S,t)$ with respect to S and t represent the rates of change of $\mathbf{t_I}(S,t)$ and are defined by:

$$\frac{\partial \mathbf{R}(S,t)}{\partial S} = \hat{\boldsymbol{\omega}}(S,t) \cdot \mathbf{R}(S,t) = \mathbf{R}(S,t) \cdot \hat{\boldsymbol{\Omega}} \tag{2}$$

$$\frac{\partial \mathbf{R}(S,t)}{\partial t} = \hat{\mathbf{w}}(S,t)\cdot\mathbf{R}(S,t) = \mathbf{R}(S,t)\cdot\hat{\mathbf{W}} \tag{3}$$

where $\hat{\boldsymbol{\omega}}$ and $\hat{\mathbf{w}}$ are skew-symmetric tensors defining the spatial curvature and rotational velocity of a configuration, while $\hat{\boldsymbol{\Omega}}$ and $\hat{\mathbf{W}}$ are the corresponding material tensors.

2.2 Equilibrium equations

The spatial form of the linear and angular momentum equations is given by:

$$\begin{aligned} &\frac{\partial \mathbf{n}}{\partial S} + \bar{\mathbf{n}} = \rho A \ddot{\mathbf{x}}_0 \\ &\frac{\partial \mathbf{m}}{\partial S} + \frac{\partial \mathbf{x}_0}{\partial S}\times\mathbf{n} + \bar{\mathbf{m}} = \rho\mathbf{I}\cdot\dot{\mathbf{w}} + \mathbf{w}\times(\rho\mathbf{I}\cdot\mathbf{w}) \end{aligned} \tag{4}$$

In Eq. (4) $\mathbf{n}$ and $\mathbf{m}$ are the spatial force and moment resultants while $\bar{\mathbf{n}}$ and $\bar{\mathbf{m}}$ are the distributed applied forces and moments per unit length of the beam. Moreover, A and $\mathbf{I}$ are the area and spatial inertia tensor of the cross-section, ρ is the mass density and $\mathbf{w}$ is the spatial rotational velocity vector.

2.3 Constitutive equations

Large deformations but locally small strains are assumed so that forces and moments are linearly proportional to the corresponding strains and curvatures through a constant elasticity tensor **C.** The following expressions hold:

$$\mathbf{C} = \mathrm{diag}\left[GA_1, GA_2, EA, EI_1, EI_2, GJ_t\right] \tag{5}$$

$$\begin{bmatrix}\mathbf{N}\\ \mathbf{M}\end{bmatrix} = \mathbf{C}\begin{bmatrix}\boldsymbol{\Gamma}\\ \boldsymbol{\Omega}\end{bmatrix} \tag{6}$$

where $\mathbf{N} = \mathbf{R}^{\mathbf{T}}\cdot\mathbf{n}$ and $\mathbf{M} = \mathbf{R}^{\mathbf{T}}\cdot\mathbf{m}$ are the material force and moment resultants, while $\boldsymbol{\Gamma}$ and $\boldsymbol{\Omega}$ are the corresponding strains and curvatures defined as:

$$\begin{aligned} \boldsymbol{\Gamma} &= \mathbf{R}^{\mathbf{T}}\cdot\frac{\partial \mathbf{x}_0}{\partial S} - \mathbf{E}_3 \\ \boldsymbol{\Omega} &= \mathbf{R}^{\mathbf{T}}\cdot\boldsymbol{\omega} \end{aligned} \tag{7}$$

where $\boldsymbol{\omega}$ is the spatial curvature vector.

3 WEAK FORM OF THE EQUILIBRIUM EQUATIONS

Following Simo [3,4], the weak form of the equilibrium equations is obtained by multiplying the spatial balance equations (4) by an admissible variation $\boldsymbol{\eta} = (\mathbf{u}_0, \boldsymbol{\theta})$:

$$\begin{aligned} G(\mathbf{x},\boldsymbol{\eta}) = &\int_0^L \left[\left(\frac{\partial \mathbf{n}}{\partial S} + \bar{\mathbf{n}}\right)\cdot\mathbf{u}_0 + \left(\frac{\partial \mathbf{m}}{\partial S} + \frac{\partial \mathbf{x}_0}{\partial S}\times\mathbf{n} + \bar{\mathbf{m}}\right)\cdot\boldsymbol{\theta}\right] dS + \\ &-\int_0^L \left\{\rho A\ddot{\mathbf{x}}_0\cdot\mathbf{u}_0 + \left[\rho\mathbf{I}\cdot\dot{\mathbf{w}} + \mathbf{w}\times(\rho\mathbf{I}\cdot\mathbf{w})\right]\cdot\boldsymbol{\theta}\right\} dS = 0 \end{aligned} \tag{8}$$

If $\boldsymbol{\varphi}(S,t)=\left[\mathbf{x}_0(S,t),\mathbf{R}(S,t)\right]$ represents an arbitrary configuration, $\mathbf{u}_0$ can be interpreted as a superposed infinitesimal displacement on the line of centroids $\mathbf{x}_0$, and $\boldsymbol{\theta}$ as a superposed infinitesimal rotation onto the moving frame defined by $\mathbf{R}$. More precisely, $\boldsymbol{\theta}$ represents the axial vector of the skew-symmetric tensor $\hat{\boldsymbol{\theta}}$. It should be noted that by exponentiation of the incremental rotation tensor $\hat{\boldsymbol{\theta}}$ we are guaranteed to obtain an orthogonal tensor representing a finite rotation.

Integration by parts of the first integral of Eq. (8) leads to the following spatial version of the weak form of the equilibrium equations:

$$\begin{aligned} G(\boldsymbol{\varphi},\boldsymbol{\eta}) &= \int_0^L \left[\mathbf{n}\cdot\left[\frac{\partial \mathbf{u}_0}{\partial S}-\boldsymbol{\theta}\times\frac{\partial \mathbf{x}_0}{\partial S}\right]+\mathbf{m}\cdot\frac{\partial \boldsymbol{\theta}}{\partial S}\right]dS-\int_0^L\left(\bar{\mathbf{n}}\cdot\mathbf{u}_0+\bar{\mathbf{m}}\cdot\boldsymbol{\theta}\right)dS \\ &+\int_0^L\left\{\rho A\ddot{\mathbf{x}}_0\cdot\mathbf{u}_0+\left[\rho\mathbf{I}\cdot\dot{\mathbf{w}}+\mathbf{w}\times\left(\rho\mathbf{I}\cdot\mathbf{w}\right)\right]\cdot\boldsymbol{\theta}\right\}dS=0 \end{aligned} \tag{9}$$

The material version of the weak form can be easily obtained as:

$$\begin{aligned} G(\boldsymbol{\varphi},\boldsymbol{\eta}) &= \int_0^L \left[\mathbf{N}\cdot\mathbf{R}^{\mathrm{T}}\cdot\left[\frac{\partial \mathbf{u}_0}{\partial S}-\boldsymbol{\theta}\times\frac{\partial \mathbf{x}_0}{\partial S}\right]+\mathbf{M}\cdot\mathbf{R}^{\mathrm{T}}\cdot\frac{\partial \boldsymbol{\theta}}{\partial S}\right]dS-\int_0^L\left(\bar{\mathbf{n}}\cdot\mathbf{u}_0+\bar{\mathbf{m}}\cdot\boldsymbol{\theta}\right)dS \\ &+\int_0^L\left\{\rho A\ddot{\mathbf{x}}_0\cdot\mathbf{u}_0+\mathbf{R}\cdot\left[\rho\mathbf{J}\cdot\dot{\mathbf{W}}+\mathbf{W}\times\left(\rho\mathbf{J}\cdot\mathbf{W}\right)\right]\cdot\boldsymbol{\theta}\right\}dS=0 \end{aligned} \tag{10}$$

In Eq. (10) $\mathbf{J}=\mathbf{R}^{\mathrm{T}}\cdot\mathbf{I}\cdot\mathbf{R}$ is the material time-independent inertia tensor.

3.1 Time integration algorithm

Given the configuration $\boldsymbol{\varphi}_{\mathbf{n}}\left(\mathbf{x}_{0,\mathbf{n}},\mathbf{R}_{\mathbf{n}}\right)$ at time t_n, the problem of finding the configuration $\boldsymbol{\varphi}_{\mathbf{n+1}}\left(\mathbf{x}_{0,\mathbf{n+1}},\mathbf{R}_{\mathbf{n+1}}\right)$ at time t_{n+1} is dealt with as follows. As far as the translational part of the configuration is concerned the classical Newmark algorithm is used, whereas an extension of Newmark's algorithm to the orthogonal group SO(3) is considered for the rotational part of the configuration. The time integration algorithm proposed by Simo [4] is summarized below. For the translational part we have:

$$\mathbf{d}_{\mathbf{n+1}}=\mathbf{d}_{\mathbf{n}}+\mathbf{u}_{\mathbf{n}} \tag{11}$$

$$\mathbf{u}_{\mathbf{n}}=h\dot{\mathbf{d}}_{\mathbf{n}}+h^2\left[\left(\frac{1}{2}-\beta\right)\ddot{\mathbf{d}}_{\mathbf{n}}+\beta\ddot{\mathbf{d}}_{\mathbf{n+1}}\right] \tag{12}$$

$$\dot{\mathbf{d}}_{\mathbf{n+1}}=\dot{\mathbf{d}}_{\mathbf{n}}+h\left[(1-\gamma)\ddot{\mathbf{d}}_{\mathbf{n}}+\gamma\ddot{\mathbf{d}}_{\mathbf{n+1}}\right] \tag{13}$$

where we have introduced $\mathbf{d}=\mathbf{x}_0$ just to simplify the notation.

For the rotational part of the configuration the extension of Newmark's algorithm to SO(3) is given in material form by:

$$\mathbf{R}_{\mathbf{n+1}}=\mathbf{R}_{\mathbf{n}}\cdot\exp\left(\hat{\boldsymbol{\Theta}}_{\mathbf{n}}\right)=\exp\left(\hat{\boldsymbol{\theta}}_{\mathbf{n}}\right)\cdot\mathbf{R}_{\mathbf{n}} \tag{14}$$

$$\boldsymbol{\Theta}_{\mathbf{n}} = h\mathbf{W}_{\mathbf{n}} + h^2\left[\left(\frac{1}{2}-\beta\right)\dot{\mathbf{W}}_{\mathbf{n}} + \beta\dot{\mathbf{W}}_{\mathbf{n+1}}\right] \tag{15}$$

$$\mathbf{W}_{\mathbf{n+1}} = \mathbf{W}_{\mathbf{n}} + h\left[(1-\gamma)\dot{\mathbf{W}}_{\mathbf{n}} + \gamma\dot{\mathbf{W}}_{\mathbf{n+1}}\right] \tag{16}$$

In order to avoid singularities in the update of the rotation tensor, the exponentiation of the rotation tensor in the first of Eq. (14) is performed using a quaternion parameterization. The incremental material rotation vector $\boldsymbol{\Theta}_{\mathbf{n}}$ is then extracted by means of Spurrier's algorithm [3,6].

3.2 Linearization and space discretization of the weak form

The linear part of the material version of the weak form of the equilibrium equations (10) is given by:

$$L\left[G\left(\boldsymbol{\varphi}_{\mathbf{n+1}}, \boldsymbol{\eta}\right)\right] = G\left(\boldsymbol{\varphi}_{\mathbf{n+1}}, \boldsymbol{\eta}\right) + DG\left(\boldsymbol{\varphi}_{\mathbf{n+1}}, \boldsymbol{\eta}\right)\cdot\boldsymbol{\Delta}\mathbf{u} \tag{17}$$

In Eq. (17) $G\left(\boldsymbol{\varphi}_{\mathbf{n+1}}, \boldsymbol{\eta}\right)$ represents the unbalanced force at configuration $\left(\boldsymbol{\varphi}_{\mathbf{n+1}}, \boldsymbol{\eta}\right)$ while the term $DG\left(\boldsymbol{\varphi}_{\mathbf{n+1}}, \boldsymbol{\eta}\right)\cdot\boldsymbol{\Delta}\mathbf{u}$ leads to the definition of a tangent operator. As shown by Simo [3,4], space discretization of the linearized weak form yields the following system of equations:

$$\sum_{\mathrm{I,J=1}}^{\mathrm{N}}\left[\mathbf{P}_{\mathbf{I}}\left(\boldsymbol{\varphi}_{\mathbf{n+1}}\right) + \mathbf{K}_{\mathbf{IJ}}\left(\mathbf{R}_{\mathbf{n}}, \boldsymbol{\varphi}_{\mathbf{n+1}}\right)\boldsymbol{\Delta}\mathbf{u}_{\mathbf{J,n+1}}\right] = \mathbf{0} \tag{18}$$

where N is the number of discretization nodes, $\boldsymbol{\Delta}\mathbf{u}_{\mathbf{j,n+1}}$ represents the incremental displacement-rotation field and the tangent matrix $\mathbf{K}$ is given by the sum of the material stiffness matrix **S**, the geometric stiffness matrix **G** and the inertia matrix $\bar{\mathbf{M}}$, that is

$$\mathbf{K}_{\mathbf{IJ}} = \mathbf{S}_{\mathbf{IJ}} + \mathbf{G}_{\mathbf{IJ}} + \bar{\mathbf{M}}_{\mathbf{IJ}} \tag{19}$$

Expressions for the above matrices can be found in [3,4]. The system of equations (18) is solved by means of an iterative scheme of the Newton type. Details of the solution scheme, as well as of the linearization and discretization of the weak form can also be found in [3,4].

4 NUMERICAL APPLICATIONS

In this section the three-dimensional geometrically exact beam model is applied to describe the behavior of an electrical conductor tested at the University at Buffalo [5]. The cable considered is a Jefferson/TW AAC conductor made of 52 helically wrapped aluminum wires. All the numerical applications are performed using MATLAB.

4.1 Properties of the cable

The material properties used in the analyses are E=10x10^6 psi and $\nu = 0.33$, whereas the geometric properties of the cable are L=145 in, A=2.07 in^2, I_1=I_2=0.0068 in^4 and J_t=I_1+I_2. The weight of the cable is 0.188 lbs/in.

It is usually difficult to evaluate the effective moment of inertia of cables based on the geometry of the cross section only, as considerably different values can be obtained depending on whether the wires remain connected or can more or less slide with respect to one another during bending. The value taken herein was chosen to yield a good matching of the in-plane and out-of-plane fundamental frequencies measured during the experimental tests. Once the

static shape of the cable has been found numerically, its frequencies are estimated by linear eigenvalue analysis using the tangent stiffness matrix at the given configuration and an appropriate consistent mass matrix.

4.2 Cable form finding

The first application is concerned with determining the static configuration of the cable from which the dynamic tests were performed. This is obtained by imposing end displacements and rotations to an initially straight and unstrained cable. The conductor is discretized using 80 2-noded (linear) elements with 1-point Gaussian integration. The shape of the cable obtained by the numerical model is plotted in Figure 1 against the initial configuration measured prior to the dynamic experiments.

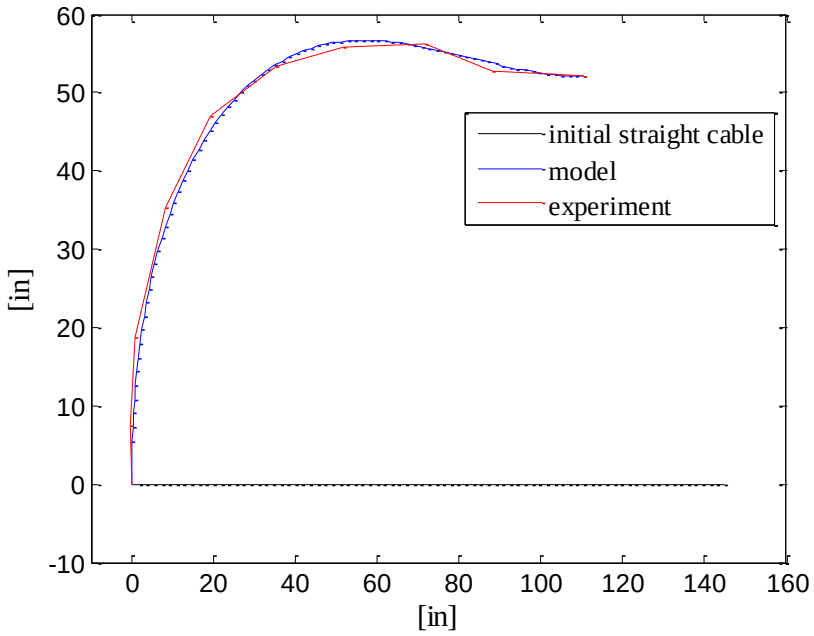

Figure 1: Numerical and experimental static configuration of the cable.

4.3 Response to harmonic ground motion

Starting from the configuration obtained in the previous section, the dynamic performance of the algorithm is tested by separately applying in-plane and out-of-plane horizontal harmonic displacements at the ends of the cable in the form:

$$u(t) = U \sin(2\pi ft) \tag{20}$$

where U and f are the amplitude and frequency of the applied motion.

4.4 Resonant responses

In the present applications displacement amplitudes of 1 inch are considered and the exciting frequencies are taken equal to the fundamental natural frequencies of the cable. These are 1.5 Hz for the out-of-plane motion and 4.15 Hz for the in-plane motion. The parameters used in the time integration scheme are $\beta = 0.25$ and $\gamma = 0.5$. A time step $\Delta t = 0.001$s is used for the out-of-plane excitation while $\Delta t = 0.0001$ s is used for the in-plane application. Small time steps are needed to avoid instability problems due to high frequency effects related to the

axial response of the cable. Moreover, it is known that the Newmark family of time-integration algorithms generally fails to conserve energy and can lead to unstable and inaccurate results. For this reason algorithms have been proposed in the literature, which introduce numerical damping to stabilize the computations [7,8]. In this paper we do not implement these algorithms but the introduction in the model of real forms of damping is object of current work.

For both the out-of-plane and the in-plane excitations, the first 10 seconds of motion are analyzed. 1-point Gaussian integration is used for the internal force vector and the material and geometric stiffness matrices, while 2-point Gaussian integration is used for the inertial force vector and the inertia matrix.

The components of the response of a reference point along the cable to the out-of-plane excitation are shown in Figure 2, along with the deformed shape of the cable at the time of maximum out-of plane horizontal displacement. The reference point is marked in Figure 2(d). It should be noted that the vertical displacements are of the same magnitude as the out-of-plane horizontal ones.

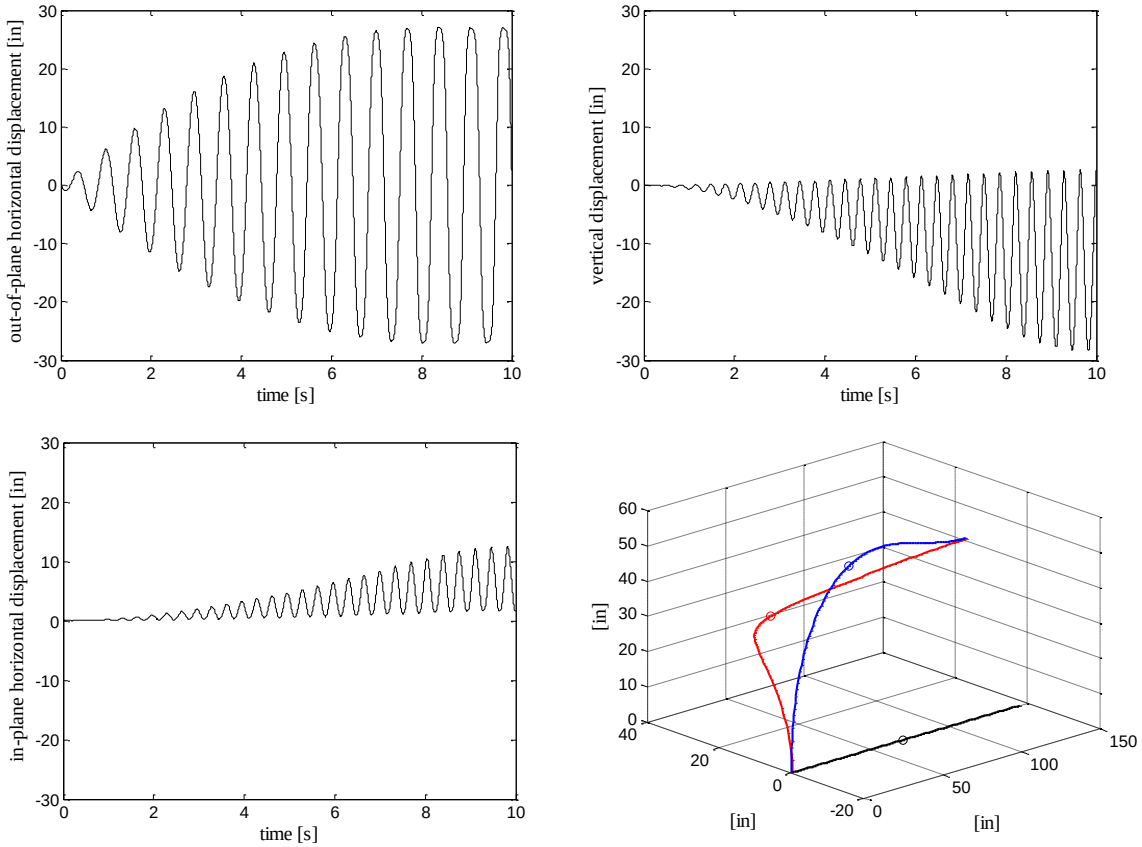

Figure 2: Numerical response of reference point to out-of-plane resonant excitation. (a) Out-of-plane horizontal displacement, (b) vertical displacement, (c) in-plane horizontal displacement, (d) deformed shape at maximum out-of-plane displacement.

The components of the response of the reference point due to the in-plane excitation are shown in Figure 3, along with the deformed shapes of the cable at the time of maximum vertical and horizontal displacements. It should be noted that in the case of in-plane horizontal excitation the cable undergoes no out-of-plane displacements.

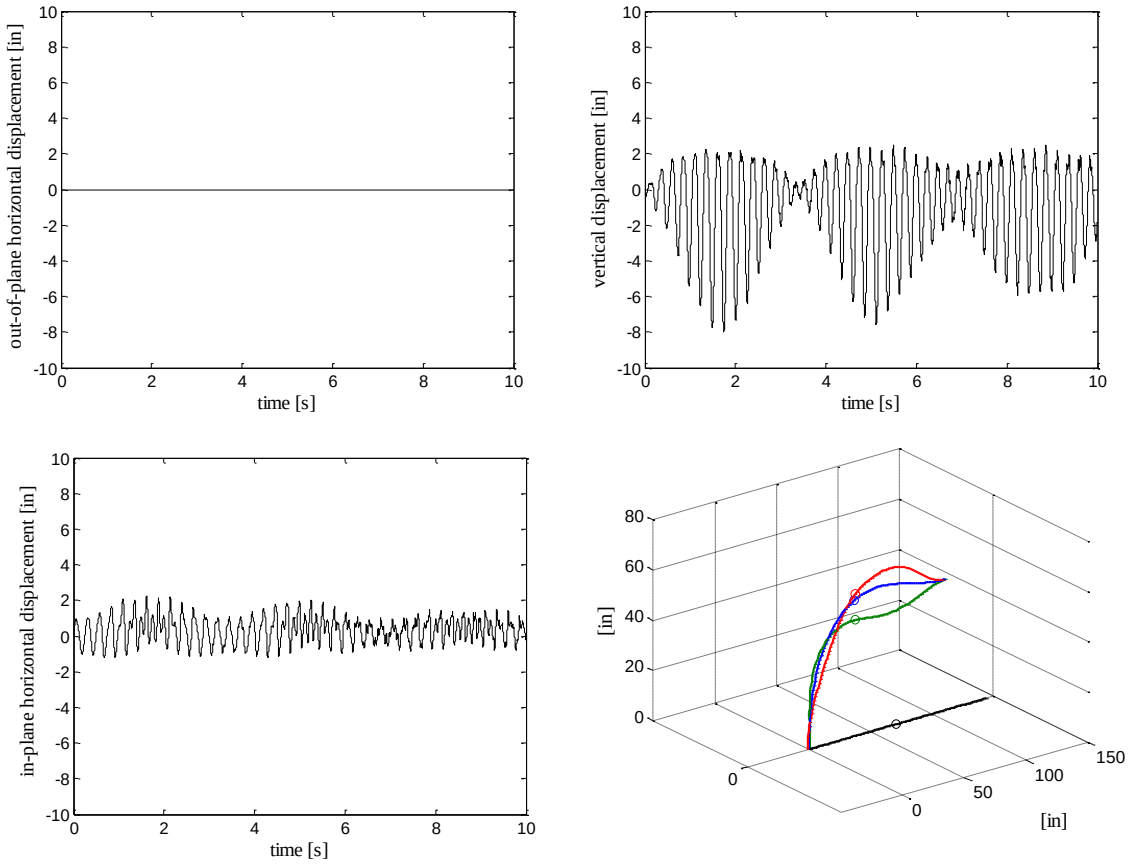

Figure 3: Numerical response of reference point to in-plane resonant excitation. (a) Out-of-plane horizontal displacement, (b) vertical displacement, (c) in-plane horizontal displacement, (d) deformed shape at maximum and minimum vertical displacements.

5 CONCLUSIONS

A three-dimensional geometrically exact beam model has been presented for the static and dynamic behavior of electrical equipment cables. The model has been implemented in MATLAB and applied to a flexible conductor tested at the SEESL lab at the University at Buffalo. The performance of the numerical algorithm has been evaluated through static and dynamic applications in the form of harmonic ground excitations. The results show that further investigation is needed to assess the accuracy and stability of the computations. The introduction of different forms of damping in the model and the simulation of the dynamic experimental tests performed at the University at Buffalo are object of current work.

REFERENCES

[1] K.J. Hong, A. Der Kiureghian, J.L. Sackman, Seismic Interaction in Cable-Connected Equipment Items. *Journal of Engineering Mechanics*, **127**(11), 1096-1105, 2001.

[2] J.C. Simo, A finite strain beam formulation. The three-dimensional dynamic problem. Part I. *Computer Methods in Applied Mechanics and Engineering*, **49**, 55-70, 1985.

[3] J.C. Simo, L. Vu-Quoc, A three-dimensional finite-strain rod model. Part II: Computational aspects. *Computer Methods in Applied Mechanics and Engineering*, **58**, 79-116, 1986.

[4] J.C. Simo, L. Vu-Quoc, On the dynamics in space of rods undergoing large motions - a geometrically exact approach. *Computer Methods in Applied Mechanics and Engineering*, **66**, 125-161, 1988.

[5] P. Chandran, Experimental and numerical studies on the seismic response of flexible conductors with vertical drops. *Master of Science Project Report*, University at Buffalo, NY, 2012.

[6] R.A. Spurrier, Comment on "singularity-free extraction of a quaternion from a direction-cosine matrix", *J. Spacecraft*, **15 (4)**, 255, 1978.

[7] J. C. Simo, N. Tarnow, K. K. Wong, (1992), Exact energy-momentum conserving algorithms and symplectic schemes for nonlinear dynamics. *Computer Methods in Applied Mechanics and Engineering*, **100 (1)**, 63-116, 1992.

[8] J. C. Simo, N. Tarnow, M. Doblare, Nonlinear dynamics of three-dimensional rods: Exact energy and momentum conserving algorithms. *International Journal of Numerical Methods in Engineering*, **38 (9)**, 1431-1473, 1995.